

# Patho-R1: A Multimodal Reinforcement Learning-Based Pathology Expert Reasoner

Wenchuan Zhang<sup>1,2\*</sup> Penghao Zhang<sup>3\*</sup> Jingru Guo<sup>4\*</sup> Tao Cheng<sup>5</sup> Jie Chen<sup>2</sup>  
Shuwan Zhang<sup>6</sup> Zhang Zhang<sup>1</sup> Yuhao Yi<sup>1,2†</sup> Hong Bu<sup>1,2</sup>

<sup>1</sup>Department of Pathology, West China Hospital, Sichuan University

<sup>2</sup>Institute of Clinical Pathology, West China Hospital, Sichuan University

<sup>3</sup>Independent Researcher <sup>4</sup>University of Toronto <sup>5</sup>Business School, Sichuan University

<sup>6</sup>Department of Pathology, Shengjing Hospital of China Medical University  
zhangwenchuan@stu.scu.edu.cn, yuhaoyi@scu.edu.cn

## Abstract

Recent advances in vision-language models (VLMs) have enabled broad progress in the general medical field. However, pathology still remains a more challenging sub-domain, with current pathology-specific VLMs exhibiting limitations in both diagnostic accuracy and reasoning plausibility. Such shortcomings are largely attributable to the nature of current pathology datasets, which are primarily composed of image-description pairs that lack the depth and structured diagnostic paradigms employed by real-world pathologists. In this study, we leverage pathology textbooks and real-world pathology experts to construct high-quality, reasoning-oriented datasets. Building on this, we introduce Patho-R1, a multimodal RL-based pathology Reasoner, trained through a three-stage pipeline: (1) continued pretraining on 3.5 million image-text pairs for knowledge infusion; (2) supervised fine-tuning on 500k high-quality Chain-of-Thought samples for reasoning incentivizing; (3) reinforcement learning using Group Relative Policy Optimization and Decoupled Clip and Dynamic sAmpling Policy Optimization strategies for multimodal reasoning quality refinement. To further assess the alignment quality of our dataset, we propose PathoCLIP, trained on the same figure-caption corpus used for continued pretraining. Comprehensive experimental results demonstrate that both PathoCLIP and Patho-R1 achieve robust performance across a wide range of pathology-related tasks, including zero-shot classification, cross-modal retrieval, Visual Question Answering, and Multiple Choice Question. Our project is available at the Patho-R1 repository: <https://github.com/Wenchuan-Zhang/Patho-R1>.

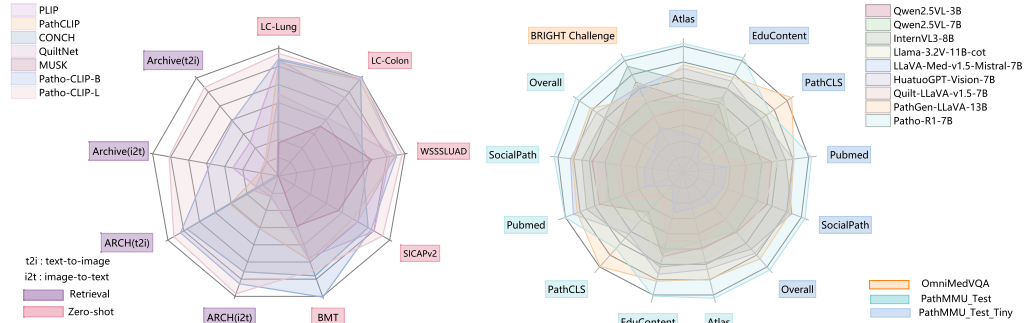


Figure 1: The performance of the proposed PathoCLIP (left), and the Patho-R1 (right).

\*Equal contribution.

†Corresponding author.

# 1 Introduction

In the medical domain, pathology, as the gold standard of modern clinical diagnosis [1], plays a pivotal role in guiding therapeutic decisions [2]. However, building robust AI systems for pathology presents significantly greater challenges compared to other medical imaging tasks like MRI [3] or CT [4]. This stems from the inherent complexity and fine-grained nature of pathology data, coupled with the scarcity of high-quality, expert-annotated multimodal datasets [5]. While general vision-language models (VLMs), such as CLIP [6] and LLaVA [7], have shown promising results across various medical imaging tasks [8, 9, 10], their performance in pathology remains limited—especially in terms of cross-disease generalization and the comprehension of complex diagnostic tasks—highlighting the urgent need for pathology-specific solutions [11, 12, 13].

To address this gap, recent efforts [14, 15] introduced pathology-adapted multimodal datasets [16, 17, 15], demonstrating impressive performance on various benchmark tasks, facilitating the initial transformation of generic multimodal architectures to the pathology domain. However, despite their competitive results on constrained tasks such as Multiple Choice Question (MCQ) and Visual Question Answering (VQA), the underlying decision-making principles of the models remain opaque, limiting their applicability in real-world clinical settings, where interpretability and trustworthiness are critical for deployment. Existing datasets, constructed from educational videos, social media posts, and institutional archives share a common characteristic: the pairing between visual and textual modalities tends to privilege surface-level descriptions over semantically rich, diagnostically grounded interpretations. “Textbook-quality” data [18], encompassing detailed disease mechanisms and organized domain knowledge, may predictably yield a model’s capacity for clinically grounded reasoning.

Notably, recent success in reinforcement learning, exemplified by DeepSeek-R1 [19], QwQ-32B [20], Kimi k1.5 [21], have revealed the strong potential of reinforcement learning in fostering reasoning abilities within language models. Among existing methods, the Group Relative Policy Optimization (GRPO) stands out for its simple but effective ground truth-driven reward design. Numerous subsequent works continuously validate its capability, not only in logic-intensive tasks like math and coding, but in domains that, while less dependent on symbolic deduction, require systematic thinking and structured judgement instead [22, 23, 24, 25]. More intriguingly, recent works have pushed GRPO forward: the Decoupled Clip and Dynamic sAmpling Policy Optimization (DAPO) [26] leverages higher clip ratio and dynamically sampled training batches to yield promising performance with fewer training steps, offering an inspiring alternative to domain-aligned reward mechanism design.

Specifically, our key contributions include:

- We propose a comprehensive **data curation pipeline** that requires **minimal human effort** while ensuring scalable generation of **high-quality SFT data with reasoning**.
- We present ***PathoCLIP***, an open-source pathology adapted CLIP model, which outperforms state-of-the-art models in classification and retrieval tasks.
- We explore the end-to-end training process of domain adaptation of pretrained vision-language models, especially the latest reinforcement learning methods: **GRPO** and **DAPO**. We release the model weights of our vision-language pathology reasoning model: ***Patho-R1***, which demonstrates superior performance on various benchmarks as shown in Figure 1.

## 2 Related Work

**Large Vision Language Models in Medical Fields.** The emergence of general-purpose VLMs such as CLIP [6] has significantly advanced the development of multimodal models in the medical domain. To better capture domain-specific semantics, various CLIP-based adaptations have been proposed, including PubMedCLIP [27], MedCLIP [8], BiomedCLIP [28], PMC-CLIP [11], UniMed-CLIP [29], and Med-PaLM [30]. These models leverage large-scale medical image-text pairs for contrastive pretraining, leading to improved performance on tasks such as medical image classification and retrieval. To further enhance the utility of medical VLMs, a new line of multimodal medical assistants has emerged, including BiomedGPT [12], Med-Flamingo [9], LLaVA-Med [13], RadFM [10], and HuatuoGPT-Vision [31]. These models integrate large language models to enable image-conditioned

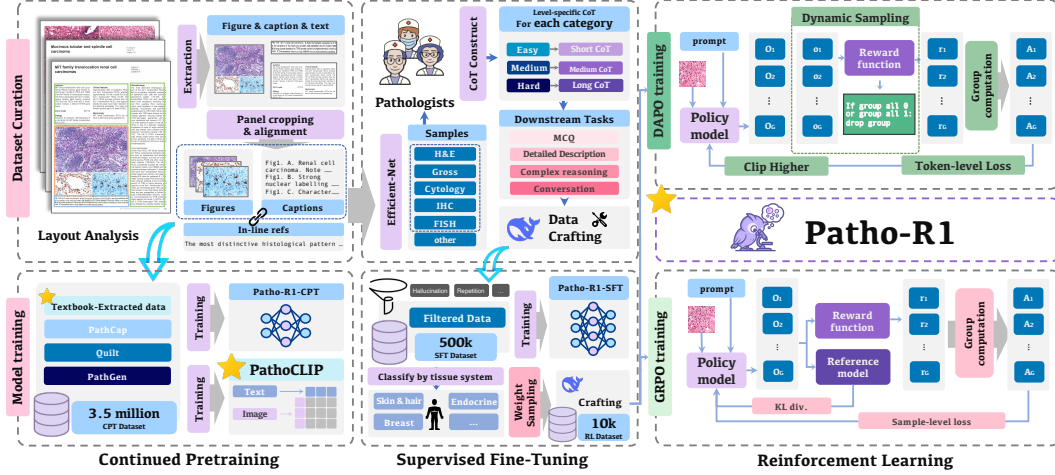


Figure 2: The sequential pipeline for developing Patho-R1. We start by extracting and aligning figures, captions, and in-line references. The image caption pairs, combined with public datasets, will be used for Patho-CLIP training and CPT for Patho-R1 training. Pairs with in-line references will be categorized into pathological sub-fields, clustered by difficulty, applied into tasks with level-specific CoTs to construct SFT data. Data with diagnosis information will be sampled for the final RL.

dialogue and question answering, aiming to support more interactive and context-aware medical understanding. In the field of pathology, where challenges such as extremely high-resolution images and subtle morphological distinctions prevail, several domain-specific CLIP-structured models have been developed, including PLIP [17], CONCH [32], MUSK [33], TITAN [34], and QuiltNet [16]. Alongside these, a growing number of pathology-focused multimodal models have been introduced, such as PathAsst [35], Quilt-LLaVA [14], PathChat [36], CPath-Omni[37], PathGen-LLaVA [15], and PA-LLaVA [38]. These models attempt to adapt general-purpose architectures to the pathology domain and incorporate capabilities such as visual question answering and multi-turn dialogue to facilitate diagnostic support.

**Vision-Language Reinforcement Learning for Post-Training.** Recently, the focus of large language model (LLM) research has been shifting from traditional supervised learning to reinforcement learning (RL) as a means to enhance reasoning capabilities [19, 39]. One line of work centers around Chain-of-Thought (CoT) prompting: it involves constructing structured multimodal reasoning datasets and performing instruction tuning to improve the model’s reasoning traceability, as seen in LLaVA-CoT [40] and LlamaV-o1 [41]. In contrast, another class of approaches, such as Visual-RFT [42], VLM-R1 [43], and Perception-R1 [44], bypasses CoT-style instruction tuning and instead focuses on leveraging RL to directly enhance visual perception. These methods typically rely on carefully designed reward functions to guide models toward learning more robust visual representations under unsupervised or weakly supervised conditions. A further evolution of this line of work is exemplified by R1-OneVision [45], R1-V [46], and Vision-R1 [22], which propose a novel cross-modal reasoning pipeline. These methods first convert images into formalized language representations that encapsulate visual semantics, then construct language-centric visual reasoning datasets for instruction tuning, followed by an RL phase to incentivize deeper multimodal reasoning. Although these methods have made significant progress in general fields, their exploration in the field of medical imaging is still in its early stages. For example, MedVLM-R1 [24] and Med-R1 [23] have only made preliminary adaptations to medical scenarios and lack system modeling and expert knowledge guidance for specific tasks.

### 3 Method

#### 3.1 Dataset Overview

As the potential of VLMs for domain-specific applications continues to be explored, constructing high-quality datasets is increasingly crucial for developing clinically meaningful models. However,

existing datasets have two main drawbacks: (1) *Existing datasets most focus on general medical domains, leaving a gap in the collection of pathology-specific data*; (2) *They often lack detailed, authoritative, and diagnostically accurate records of the diagnostic process, focusing primarily on simple descriptions and conclusions*. To address these issues, we curated a large-scale, pathology-specific multimodal corpus covering 3 publicly available datasets, 660 authoritative pathology textbooks and education notes. The overview of our data curation and model training pipeline is shown in Figure 2. Datasets used in each training phase are described below. For more details of the training data, see Appendix A.

**Continued Pretraining (CPT):** Our CPT dataset comprises a total of **3.5 million image-text pairs**, of which 2.8 million are from PubMed [35], Quilt [16], PathGen [15], and 0.7 million from pathology textbooks and notes. This dataset also serves as the training data for our PathoCLIP.

**Supervised Fine-tuning (SFT):** Our SFT dataset comprises **500k samples** drawn from 5 pathological subfields: histopathology, gross examination, immunohistochemistry (IHC), cytology, fluorescence in situ hybridization (FISH); with 3 distinct levels of Chain-of-Thoughts per subfield; spanning 4 downstream task types: descriptive analysis, complex reasoning, multi-turn conversations, multiple-choice questions. This results in a total of 60 data combination types.

**Reinforcement Learning:** Our RL dataset comprises 10k diagnostic-oriented MCQs, aligned with the same five pathological subfields defined in the SFT stage.

### 3.2 Continued Pretraining and PathoCLIP Training

**Data Preparation.** We first scanned pathology textbooks into high-resolution images and used DocLayoutYolo [47] to segment each page into body text, figure panels, and captions. Figure-caption pairs were matched based on spatial layout, and captions were extracted using OCR. For multi-panel figures, we applied edge detection and label recognition to split composite images and align sub-figures with corresponding caption segments. To leverage the rich contextual information in textbook narratives, we also extracted body text via OCR and used the Qwen-max model to automatically identify in-line references between figures and surrounding text, reducing the need for manual annotation. Further details are provided in Appendix A.2.

**PathoCLIP Training.** We employ OpenAI-CLIP-B and OpenAI-CLIP-L as backbone architectures of our model. To construct a cross-modal model endowed with both fine-grained morphological representation and clinical pathology comprehension capabilities, we implement a two-stage progressive training paradigm inspired by [15]: in stage I, we initialize the model via contrastive learning on the PathGen-1.6M dataset, which emphasizes tissue-cell morphology and spatial organization to instill high-resolution morphological priors; in stage II, we preserve these morphological representations while integrating PathGen-1.6M with Quilt-1M, PathCap, and our textbook-extracted dataset, yielding a composite corpus of 3.5 million image-text pairs. Empirical evaluations demonstrate that this progressive strategy not only significantly enhances the model’s ability to discriminate tissue heterogeneity but achieves state-of-the-art semantic understanding and image-text retrieval performance on a range of pathological diagnostic benchmarks. For more details on PathoCLIP training, see Appendix B.1.

**Patho-R1 Continued Pretraining.** Continued Pretraining has been empirically validated to be an effective approach to inject domain-specific knowledge into pretrained language models [48], as well as achieve competitive or even superior performance compared to larger-scale models [31]. To ensure a wide coverage of pathological knowledge, we incorporated all publicly available pathology datasets with our retrieved context-rich image-caption pairs. Given that the total dataset contains 3.5 million samples, we selected Qwen2.5VL-3B and Qwen2.5VL-7B as our base models to balance model capacity and data volume.

### 3.3 Invoking Reasoning Ability via SFT

Continued pretraining on domain-specific corpora can endow the model with domain knowledge, but hurt its instruction following ability [49]. During this phase, our intentions are: (1) *recovering the model’s instruction-following ability*; (2) *invoking reasoning behavior tailored to pathological diagnostics*. Unlike general-domain data, pathological diagnosis is highly structured—real-world pathologists typically follow a systematic process when interpreting histological images. Hence, a



cost-effective data generation strategy that balances data granularity with diagnostic specificity is crucial for this training phase.

We started by categorizing textbook-extracted image-caption pairs into pathology subfields. A small subset of data was manually labeled to serve as supervision for training an EfficientNet-based [50] classifier. Batched inference results on the unlabeled data were manually inspected and corrected before being incorporated into the training set to iteratively boost classifier training. Among the 10 initially identified subfields, we chose 5 with the largest data volume and highest pathological relevance as candidate subfields for SFT: histopathology, gross examination, IHC, cytology and FISH. However, five subfields were still far from meeting the requirement of data diversity. To address this, inspired by [51], we performed a three-way K-means clustering within each subfield based on the joint embeddings of images and captions. Interestingly, we observed consistent difficulty-level distinctions among the resulting clusters, based on which we designed 3 levels of CoT reasoning: easy, medium and hard. Finally, we combined the 15 distinct CoTs with 4 types of downstream tasks: MCQ, detailed description, complex reasoning, and multi-turn conversation, yielding a total of 60 prompts for SFT data generation. For more details on SFT data generation, see Appendix A.3.

We selected DeepSeek-R1 as our SFT data generation model, primarily for the following two reasons. First, as existing VLMs have not been adapted to the pathology domain, their performance in pathological imagery understanding is not satisfactory. In our experiments, providing VLMs with image-caption-CoT prompt triplets did not yield better results compared to using only captions with a strong text-only model. Second, DeepSeek-R1, as a state-of-the-art reasoning model, shows strong capabilities in multi-step thinking and long-context understanding—both of which are crucial for handling our lengthy and complex CoT-style prompts. However, this choice inevitably suffered from certain issues due to DeepSeek’s inherent weaknesses, such as language mixing in pathological terminologies and endless repetition. To mitigate generation noise, we implemented a quality control stage involving rule-based filtering and selective manual verification. The final cleaned dataset comprises 500k samples. For implementation details, see Appendix B.2.

### 3.4 Reinforcement Learning

For reinforcement learning data generation, we constructed a diagnosis-oriented MCQ dataset by selecting a non-overlapping subset of samples from the SFT data. To ensure diversity, we performed proportionate stratified sampling based on subfield distribution. For the two largest subfields that can be further categorized by tissue systems, namely histopathology and gross examination, we divided the data accordingly and performed proportional sampling within each subfield. These samples were paired with diagnosis information to generate diagnosis-oriented MCQs. For more details on data generation, see Appendix A.4.

For each training iteration, GRPO and DAPO sample  $G$  candidate output  $\{o_i\}_{i=1}^G$  from the old policy  $\pi_{\text{old}}$ , then maximize the following objectives respectively and optimize the model  $\pi_\theta$ :

$$\mathcal{J}_{\text{GRPO}}(\theta) = \mathbb{E}_{\mathbf{v} \sim P(\mathbf{V}), \{o_i\}_{i=1}^G \sim \pi_{\theta_{\text{old}}}(O|\mathbf{v})} \left[ \frac{1}{G} \sum_{i=1}^G \frac{1}{|o_i|} \sum_{t=1}^{|o_i|} (\min(r_{i,t} A_{i,t}, \text{clip}(r_{i,t}, 1-\epsilon, 1+\epsilon) A_{i,t}) - \beta D_{\text{KL}}(\pi_\theta \parallel \pi_{\text{ref}})) \right] \quad (1)$$

$$\begin{aligned} \mathcal{J}_{\text{DAPO}}(\theta) &= \mathbb{E}_{\mathbf{v} \sim P(\mathbf{V}), \{o_i\}_{i=1}^G \sim \pi_{\theta_{\text{old}}}(O|\mathbf{v})} \left[ \frac{1}{\sum_{i=1}^G |o_i|} \sum_{i=1}^G \sum_{t=1}^{|o_i|} \min(r_{i,t} A_{i,t}, \text{clip}(r_{i,t}, 1-\epsilon_{\text{low}}, 1+\epsilon_{\text{high}}) A_{i,t}) \right] \\ &\text{s.t. } 0 < \left| \{o_i \mid \text{is\_equivalent}(a, o_i)\} \right| < G. \end{aligned} \quad (2)$$

where  $A_i = (r_i - \mu_{\{r\}}) / \sigma_{\{r\}}$  denotes the group-relative advantage, which emphasizes outputs that surpass the group average for prioritized optimization.

**Reward Function Design.** We design reward functions to guide model learning from structured and accurate responses. For the **Format Reward**, we require the model to format its response

using `<think>...</think>` for intermediate reasoning steps and `<answer>...</answer>` for the final answer. A reward score of 1 is assigned if both tag pairs appear exactly once and no content exists outside these tags; otherwise, the score is 0. For the **Accuracy Reward**, the content within the `<answer>...</answer>` tags is extracted using regular expressions, and only exact matches to a valid option from the predefined set A, B, C, D, E, F are accepted. A reward score of 1 is assigned if the extracted answer matches the ground-truth label and 0 otherwise. For the **Length-Aware Penalty**, we implement a soft overlong punishment similar to the original work of DAPO. For more details on reward function design, see Appendix B.2 For GRPO, the reward function is:

$$R^{\text{GRPO}}(a_i) = \begin{cases} 0.1 \cdot R_{\text{fmt}}(a_i) + 0.9 \cdot R_{\text{acc}}(a_i), & \text{if } R_{\text{fmt}}(a_i) = 1 \wedge R_{\text{acc}}(a_i) = 1 \\ 0, & \text{otherwise} \end{cases} \quad (3)$$

Where  $R_{\text{fmt}}$  denotes the format reward and  $R_{\text{acc}}$  denotes the accuracy reward. For DAPO, the reward function is:

$$R^{\text{DAPO}}(a_i) = \begin{cases} 0.5 \cdot R_{\text{acc}}(a_i) + 0.5 \cdot R_{\text{len}}(a_i), & \text{if } R_{\text{acc}}(a_i) = 1 \wedge R_{\text{len}}(a_i) = 1 \\ -1, & \text{otherwise} \end{cases} \quad (4)$$

Where  $R_{\text{acc}}$  denotes the format reward and  $R_{\text{len}}$  denotes the length-aware penalty.

## 4 Experiments

### 4.1 Zero-shot cross-modal retrieval

We compared PathoCLIP against ten baseline CLIP variants: OpenAI-CLIP-B, OpenAI-CLIP-L, PLIP, PathCLIP, CONCH, PathGen-CLIP, PathGen-CLIP-L, QuiltNet, PubmedCLIP, and MUSK. We evaluated each model on two image–caption pairing datasets: Archive, compiled in-house from diverse pathology texts, and ARCH [52]; performance was measured using Recall@K. As shown in Table 1, on ARCH, PathoCLIP-L achieves the highest scores across all four Recall@K settings, obtaining mean i2t and t2i recalls of 62.28% and 60.33%, respectively, substantially outperforming the leading baseline, CONCH (50.71% and 52.73%); moreover, PathoCLIP-B also surpasses CONCH. In the Archive dataset, PathoCLIP-B attains mean i2t and t2i recalls of 13.34% and 13.72%, respectively, whereas PathoCLIP-L achieves 21.31% and 22.13%, far exceeding PubmedCLIP’s 9.18% and 8.51%. These results demonstrate that the latent-space alignment strategy of PathoCLIP confers state-of-the-art accuracy and robustness in cross-modal retrieval.

Table 1: Cross-modal retrieval results on the ARCH and Archive dataset. In each cell, results are displayed as “i2t / t2i” in the format (%/%). The best-performing results highlighted in bold, with the second-best underlined.

Model	ARCH (@k)						Archive (@k)					
	@1	@5	@10	@20	Aver(i2t)	Aver(t2i)	@1	@5	@10	@20	Aver(i2t)	Aver(t2i)
OpenAI-CLIP-B	0.41/0.22	1.08/1.34	1.97/2.19	3.57/3.42	1.76	1.79	1.93/1.54	4.71/4.54	6.83/6.76	10.98/11.05	6.11	5.97
OpenAI-CLIP-L	0.86/0.71	2.86/2.75	4.46/4.69	7.33/7.63	3.88	3.95	2.45/2.52	6.31/6.54	9.51/9.58	14.31/14.51	8.15	8.29
PLIP	2.31/3.27	8.07/9.15	13.24/14.21	19.79/21.58	10.85	12.05	2.03/2.25	7.42/6.41	10.72/9.67	15.54/15.69	8.93	8.51
PathCLIP	9.86/10.42	24.48/24.74	32.63/33.26	44.12/43.34	27.77	27.94	1.50/1.41	3.14/3.20	4.31/4.71	5.85/6.70	3.70	4.01
CONCH	24.07/25.63	48.29/50.22	60.04/62.43	70.42/72.62	50.71	52.73	0.03/0.10	0.26/0.36	0.52/0.59	1.21/0.98	0.51	0.51
PathGen-CLIP	14.17/14.99	34.15/32.29	45.2/41.44	56.99/51.75	37.63	35.12	0.62/0.62	1.70/1.67	2.81/2.58	3.69/4.18	2.21	2.26
PathGen-CLIP-L	18.71/17.52	40.55/35.97	52.79/46.13	63.76/56.32	43.95	38.99	1.34/1.11	2.88/2.61	4.28/4.18	6.34/6.14	3.71	3.51
QuiltNet	2.49/3.68	8.59/11.20	12.91/17.26	20.68/25.22	11.17	14.34	0.78/1.08	2.19/2.68	3.89/4.35	6.14/6.41	3.25	3.63
PubmedCLIP	0.15/0.19	0.82/1.00	1.23/1.60	1.97/2.94	1.04	1.43	2.03/2.25	7.42/6.41	10.72/9.67	16.54/15.69	9.18	8.51
MUSK	2.04/2.07	0.19/0.19	0.37/0.33	0.74/0.74	0.34	0.33	0.03/0.03	0.16/0.16	0.33/0.29	0.65/0.75	0.29	0.31
<b>Patho-CLIP-B</b>	<b>27.53/26.71</b>	<b>55.69/55.13</b>	<b>67.60/67.08</b>	<b>77.57/77.08</b>	<b>57.10</b>	<b>56.50</b>	<b>3.63/3.43</b>	<b>10.49/10.78</b>	<b>16.01/16.50</b>	<b>23.24/24.15</b>	<b>13.34</b>	<b>13.72</b>
<b>Patho-CLIP-L</b>	<b>30.73/28.20</b>	<b>61.01/59.45</b>	<b>73.92/71.91</b>	<b>83.44/81.77</b>	<b>62.28</b>	<b>60.33</b>	<b>6.27/6.14</b>	<b>17.29/18.27</b>	<b>25.62/26.93</b>	<b>36.05/37.19</b>	<b>21.31</b>	<b>22.13</b>

### 4.2 Zero-shot image classification

To demonstrate PathoCLIP’s zero-shot classification performance, we evaluated it on five pathology datasets: SICAPv2 [53], WSSSLUAD [54], LC-Lung and LC-Colon [55], and BMT [56]. For each dataset, we augmented class labels with synonyms (e.g., in LC-Colon dataset, the “colon

adenocarcinoma” class was enriched with terms such as “adenocarcinoma of the colon” and “colorectal adenocarcinoma”) and constructed category-specific text templates (e.g., “an H&E image of CLASSNAME.”, “an image of CLASSNAME.”).

Table 2: Comparison of different CLIP models on zero-shot pathology image classification datasets with accuracy (%). The top performance is highlighted in bold, with the second-best underlined.

Model	LC-Lung	LC-Colon	WSSSLUAD	SICAPv2	BMT	Average
OpenAI-CLIP-B	54.71	67.78	81.25	25.68	31.43	52.17
OpenAI-CLIP-L	70.34	70.25	76.25	15.41	26.27	51.70
PLIP	88.79	78.38	86.21	50.61	33.33	67.47
PathCLIP	86.74	96.29	91.25	39.30	34.33	69.58
CONCH	88.93	97.35	65.14	47.36	40.67	67.89
PathGen-CLIP	91.15	96.44	81.06	<u>54.15</u>	37.17	71.99
PathGen-CLIP-L	<u>91.85</u>	<u>98.30</u>	82.50	53.39	<u>47.21</u>	74.65
QuiltNet	62.73	58.15	90.50	41.85	33.83	57.41
PubmedCLIP	86.73	95.66	91.25	39.07	34.83	69.51
MUSK	25.48	49.69	72.15	31.72	20.33	39.87
<b>Patho-CLIP-B</b>	89.90	<b>98.60</b>	<u>91.80</u>	49.01	<b>49.33</b>	<u>75.28</u>
<b>Patho-CLIP-L</b>	<b>93.78</b>	97.48	<b>95.89</b>	<b>55.09</b>	38.44	<b>76.14</b>

As shown in Table 2, PathoCLIP-L surpasses CONCH by 30.75% on WSSSLUAD dataset and by 7.73% on SICAPv2 dataset, achieving the highest accuracy across all five datasets with a mean accuracy of 76.14%. Notably, on BMT dataset, PathoCLIP-B attains 49.33% accuracy—exceeding PathoCLIP-L and substantially outperforming QuiltNet (33.83%) and PathGen-CLIP (37.17%). The strong performance of PathoCLIP underscores the diversity of our pathology training data and validates our two-stage progressive training paradigm

for enhancing semantic understanding in CLIP models.

### 4.3 Few-shot image classification with linear probing

We also discuss the effectiveness of the model in few-shot learning, which is fine-tuned by linear probing of the pre-extracted feature representations of the model. We selected two representative datasets, LC-Lung and BMT, for testing under different training sizes of 2, 8, 16, 32, 64 and 128 samples, each of which implements 10 random samples. For each sample setting, we run 10 independent experiments, and finally the performance of the model under multivariate conditions is visualized by box-and-line plots.

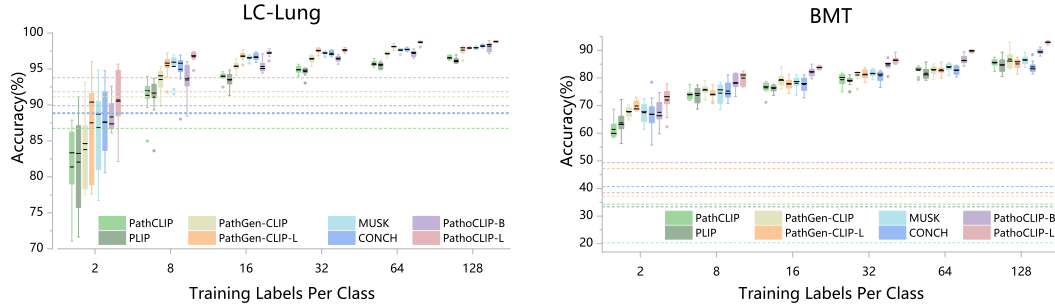


Figure 3: Comparison of few-shot classification accuracy (%) across different CLIP models on various pathology image classification datasets. For reference, the zero-shot performance of each model is shown as a dashed line on the same plot.

The experimental results show that the PathoCLIP series demonstrates excellent performance in extreme low-sample scenarios, providing a viable solution for annotation-poor clinical environments. As shown in Figure 3, on the BMT dataset, the PathoCLIP-L model achieves 73% accuracy with only 2 training samples, which is a significant advantage over the comparative models such as CONCH, PLIP, MUSK, PathGen-CLIP, etc. (none of the comparative models exceeds 70% accuracy), and the performance of the PathoCLIP-L model improves faster and converges faster as the number of training samples increases. The model outperforms comparable methods in terms of performance improvement and convergence speed as the number of training samples increases. The narrower distribution interval presented by its box-and-line plot further confirms the leading edge of the model in terms of task adaptability and robustness. Further experiments are provided in Appendix C.1.

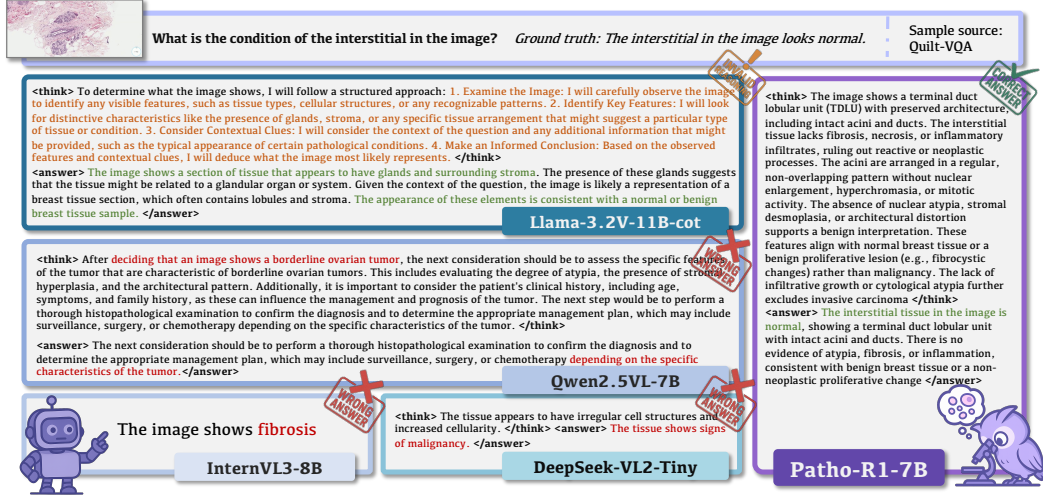


Figure 4: A representative example from the VQA task. While other models exhibit issues in answer formatting, factual accuracy, and reasoning coherence, our model consistently delivers well-structured, accurate, and logically sound responses.

## 4.4 Patho-R1 Evaluation Results

### 4.4.1 Open-ended Benchmarks

Our proposed model, Patho-R1, is designed to perform step-by-step reasoning and produce accurate final answers. As shown in Figure 4, existing general-purpose and medical models do not necessarily possess the reasoning capability required to correctly answer pathology-specific questions. To evaluate its performance, we follow a fuzzy evaluation strategy in which Deepseek-R1 acts as the LLM-judge, scoring generated outputs based on ten well-defined criteria [41]. Evaluations are conducted using the VLMEvalKit [57] framework on two publicly available pathology VQA datasets: Quilt-VQA and Path-VQA. This setup ensures consistency, reproducibility, and fair comparison with other models. Our comprehensive evaluation highlights the strength of Patho-R1 in advancing multimodal reasoning in pathology. In addition to the traditional CoT prompts, we also used the latest Chain-of-Decision (CoD) prompts [58] to explore whether simplifying the reasoning chain affects model performance. For ablation studies and other experiments, see Appendix C.2 and C.3.

Our experimental results in Figure 5 show that Patho-R1 achieves the highest accuracy on both the Quilt VQA and Path VQA open-ended question-answering datasets, while also ranking highly in reasoning quality. An interesting finding is that CoD prompts do help improve answer accuracy, especially on the relatively simpler Quilt VQA dataset, where the overall accuracy is higher.

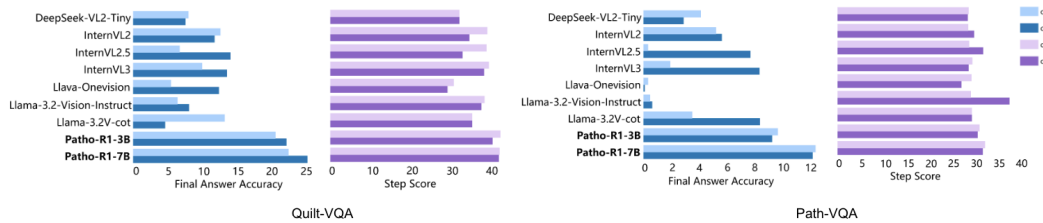


Figure 5: Evaluation of models with reasoning capabilities on final answer accuracy, coherence, and logical consistency of their reasoning steps using Quilt-VQA and Path-VQA.

### 4.4.2 Close-ended Benchmarks

Closed-ended questions play a crucial role in pathology-related tasks, particularly in diagnostic classification. To evaluate model performance on such tasks, we consider two types of close-ended

question datasets: (1) Yes/No questions, selected from PathVQA and QuiltVQA; and (2) multiple-choice questions, sourced from PathMMU [59], MedXpertQA [60], and OmniMedVQA [61]. For both types, we report accuracy as the evaluation metric to ensure consistency and comparability across datasets. Experimental results Table 3, Table 4 demonstrate that Patho-R1 outperforms previous state-of-the-art pathology-focused LMMs. Specifically, it surpasses PathGen-LLaVA-13B by 11.51 % on the PathMMU test-tiny split (PathGen-LLaVA-13B: 61.9%), by approximately 10% on the PathMMU test set, and by 5% on the PathMMU evaluation set.

Table 3: Comparison of different multimodels on PathMMU-test-tiny and PathMMU-test benchmarks. The top performance is highlighted in bold, with the second-best underlined.

Model	PathMMU-test-tiny (1139)						PathMMU-test (8454)					
	Atlas	EduContent	PathCLS	PubMed	SocialPath	Overall	Atlas	EduContent	PathCLS	PubMed	SocialPath	Overall
<b>Small model without thinking ability</b>												
Paligemma2-3b-pt-224	0.96	1.96	0	2.14	0.92	1.32	0.5	3.15	0.06	2.01	1.61	1.64
VILA1.5-3B	28.85	29.41	16.38	34.88	23.85	27.57	26.53	30.60	15.07	29.10	30.71	26.74
Llama3.2-3B-vl	30.29	27.84	7.34	27.76	30.28	25.55	35.79	25.01	6.99	25.37	28.91	23.39
<b>Large model without thinking ability</b>												
LLaVA-Med-v1.5-Mistral-7B	25.00	21.57	7.34	24.56	22.48	20.9	21.40	21.51	7.72	21.31	20.54	18.59
HuatuoGPT-Vision-7B	65.87	60.00	40.11	61.92	58.72	58.21	58.07	54.72	36.64	<u>61.36</u>	59.37	54.59
Quilt-LLaVA-v1.5-7B	42.79	38.43	14.12	37.01	32.57	33.98	41.43	36.72	14.71	34.80	35.29	32.02
PathGen-LLaVA-13B	68.27	62.35	<b>55.93</b>	62.28	59.63	61.9	63.83	58.47	<b>56.19</b>	59.24	58.47	<u>58.79</u>
<b>Small model with thinking ability</b>												
DeepSeek-VL2-Tiny	38.46	33.73	19.77	38.79	36.70	34.24	32.17	35.41	19.18	35.38	32.13	31.36
Qwen2.5VL-3B	46.63	44.31	23.73	49.82	46.79	43.37	45.06	45.28	23.65	46.79	48.10	42.10
<b>Patho-R1-3B</b>	<u>74.52</u>	<u>67.45</u>	36.72	<u>67.62</u>	<u>66.51</u>	<u>63.83</u>	<u>72.22</u>	<u>62.51</u>	34.99	61.07	<u>64.07</u>	57.93
<b>Large model with thinking ability</b>												
InternVL2-8B	46.63	50.59	21.47	49.11	51.38	45.13	43.68	44.86	23.77	44.56	45.40	40.68
InternVL2.5-8B	51.44	50.59	29.38	55.87	57.80	50.13	50.06	50.62	32.84	50.02	50.87	46.98
InternVL3-8B	58.17	54.90	42.94	57.65	60.55	55.4	54.07	50.80	39.09	54.04	53.32	50.38
Llama-3.2-11B-Vision-Instruct	45.19	38.04	29.38	39.50	41.74	39.07	41.05	37.49	26.72	38.82	39.21	36.50
Llama-3.2V-11B-cot	49.04	47.06	29.94	53.38	45.41	46.01	51.81	45.45	30.76	48.15	46.10	44.23
LLaVA-Onevision-7B	31.25	21.18	13.56	31.32	18.35	23.79	21.65	21.27	12.01	27.77	21.25	23.40
Qwen2.5VL-7B	44.23	49.41	24.86	44.84	40.83	41.88	41.18	43.20	24.82	42.77	39.67	38.67
<b>Patho-R1-7B</b>	<b>81.73</b>	<b>75.29</b>	<u>44.63</u>	<b>72.24</b>	<b>67.89</b>	<b>69.53</b>	<b>75.34</b>	<b>66.43</b>	<u>45.40</u>	<b>66.06</b>	<b>67.93</b>	<b>63.37</b>

Table 4: Comparison of different multimodels on PathMMU-val, Quilt-VQA and Path-VQA benchmarks. The top performance is highlighted in bold, with the second-best underlined.

Model	PathMMU-val (705)						YorN (3705)	
	Atlas	EduContent	PathCLS	PubMed	SocialPath	Overall	Quilt-VQA	Path-VQA
Small model without thinking ability								
Paligemma2-3b-pt-224	1.25	1.37	0.00	2.15	0.67	1.28	32.94	44.71
VILA1.5-3B	22.50	27.40	16.67	31.33	30.00	27.23	46.65	52.41
Llama3.2-3B-vl	36.25	26.03	7.29	27.90	26.00	25.25	69.39	55.44
Large model without thinking ability								
LLaVA-Med-v1.5-Mistral-7B	22.50	20.55	7.29	18.88	18.00	17.87	67.35	55.38
HuatuoGPT-Vision-7B	61.25	54.11	38.54	55.36	60.67	54.61	59.18	65.85
Quilt-LLaVA-v1.5-7B	45.00	32.88	17.71	34.33	34.67	33.05	21.28	20.76
PathGen-LLaVA-13B	67.50	60.96	50.00	59.66	53.33	58.16	47.52	45.75
Small model with thinking ability								
DeepSeek-VL2-Tiny	36.25	28.77	17.71	28.33	34.00	29.08	44.31	46.34
Qwen2.5VL-3B	52.50	45.89	28.13	51.07	44.67	45.67	40.52	43.72
Patho-R1-3B	71.25	60.27	33.33	62.66	59.33	58.44	64.14	49.29
Large model with thinking ability								
InternVL2-8B	41.25	41.10	23.96	42.92	45.33	40.28	63.56	61.36
InternVL2.5-8B	46.25	52.05	33.33	47.64	54.00	47.80	60.06	64.78
InternVL3-8B	52.50	45.89	40.63	52.36	54.00	49.79	33.82	18.56
Llama-3.2-11B-Vision-Instruct	46.25	36.30	32.29	36.05	39.33	37.45	63.27	63.50
Llama-3.2V-11B-cot	46.25	42.47	35.42	47.64	52.67	45.82	54.81	56.42
LLaVA-Onevision-7B	20.00	19.18	16.67	30.04	23.33	23.40	24.20	52.38
Qwen2.5VL-7B	43.75	34.93	29.17	39.91	42.67	38.44	52.19	41.82
Patho-R1-7B	82.50	63.01	41.67	63.95	64.67	62.98	64.72	46.97

## 5 Conclusion

In this study, we propose a comprehensive data curation pipeline for the three phases of pathology VLM training. Using this pipeline, we construct an extensive corpus containing 3.5 million image-text pairs, 500k SFT data with reasoning, and 10k MCQs for RL. Furthermore, we explore the end-to-end domain adaptation of pretrained VLMs, yielding Patho-R1 and PathoCLIP, two open-source models that contribute to the advancement of pathology-specific vision-language research and offer practical insights for future development in this domain.

**Limitations.** First, while our CPT method effectively enhances pathology-specific alignment, more advanced CPT strategies (e.g., [49, 31]) could further mitigate instruction-following degradation but were not adopted due to the high computational cost of processing large corpora. Second, although our models exhibit some generalization ability, their performance degrades on out-of-domain modalities (e.g., MRI or CT), as our training data focuses exclusively on pathology-related sources.

## References

- [1] Y. Tolkach, L. M. Wolgast, A. Damanakis, A. Prylukhin, S. Schallenberg, W. Hulla, M.-L. Eich, W. Schroeder, A. Mukhopadhyay, M. Fuchs *et al.*, “Artificial intelligence for tumour tissue detection and histological regression grading in oesophageal adenocarcinomas: a retrospective algorithm development and validation study,” *The Lancet Digital Health*, vol. 5, no. 5, pp. e265–e275, 2023.
- [2] S. Foersch, C. Glasner, A.-C. Woerl, M. Eckstein, D.-C. Wagner, S. Schulz, F. Kellers, A. Fernandez, K. Tserea, M. Kloth *et al.*, “Multistain deep learning for prediction of prognosis and therapy response in colorectal cancer,” *Nature medicine*, vol. 29, no. 2, pp. 430–439, 2023.
- [3] S. Wang, M. Safari, Q. Li, C.-W. Chang, R. L. Qiu, J. Roper, D. S. Yu, and X. Yang, “Triad: Vision foundation model for 3d magnetic resonance imaging,” *arXiv preprint arXiv:2502.14064*, 2025.
- [4] L. Wu, J. Zhuang, and H. Chen, “Voco: A simple-yet-effective volume contrastive learning framework for 3d medical image analysis,” in *Proceedings of the IEEE/CVF Conference on Computer Vision and Pattern Recognition*, 2024, pp. 22 873–22 882.
- [5] Y. Xie, C. Zhou, L. Gao, J. Wu, X. Li, H.-Y. Zhou, S. Liu, L. Xing, J. Zou, C. Xie *et al.*, “Medtrinity-25m: A large-scale multimodal dataset with multigranular annotations for medicine,” *arXiv preprint arXiv:2408.02900*, 2024.
- [6] A. Radford, J. W. Kim, C. Hallacy, A. Ramesh, G. Goh, S. Agarwal, G. Sastry, A. Askell, P. Mishkin, J. Clark *et al.*, “Learning transferable visual models from natural language supervision,” in *International conference on machine learning*. PmLR, 2021, pp. 8748–8763.
- [7] H. Liu, C. Li, Q. Wu, and Y. J. Lee, “Visual instruction tuning,” *Advances in neural information processing systems*, vol. 36, pp. 34 892–34 916, 2023.
- [8] Z. Wang, Z. Wu, D. Agarwal, and J. Sun, “Medclip: Contrastive learning from unpaired medical images and text,” in *Proceedings of the Conference on Empirical Methods in Natural Language Processing. Conference on Empirical Methods in Natural Language Processing*, vol. 2022, 2022, p. 3876.
- [9] M. Moor, Q. Huang, S. Wu, M. Yasunaga, Y. Dalmia, J. Leskovec, C. Zakka, E. P. Reis, and P. Rajpurkar, “Med-flamingo: a multimodal medical few-shot learner,” in *Machine Learning for Health (ML4H)*. PMLR, 2023, pp. 353–367.
- [10] C. Wu, X. Zhang, Y. Zhang, Y. Wang, and W. Xie, “Towards generalist foundation model for radiology by leveraging web-scale 2d&3d medical data,” *arXiv preprint arXiv:2308.02463*, 2023.
- [11] W. Lin, Z. Zhao, X. Zhang, C. Wu, Y. Zhang, Y. Wang, and W. Xie, “Pmc-clip: Contrastive language-image pre-training using biomedical documents,” in *International Conference on Medical Image Computing and Computer-Assisted Intervention*. Springer, 2023, pp. 525–536.
- [12] K. Zhang, R. Zhou, E. Adhikarla, Z. Yan, Y. Liu, J. Yu, Z. Liu, X. Chen, B. D. Davison, H. Ren *et al.*, “A generalist vision–language foundation model for diverse biomedical tasks,” *Nature Medicine*, pp. 1–13, 2024.
- [13] C. Li, C. Wong, S. Zhang, N. Usuyama, H. Liu, J. Yang, T. Naumann, H. Poon, and J. Gao, “Llava-med: Training a large language-and-vision assistant for biomedicine in one day,” *Advances in Neural Information Processing Systems*, vol. 36, pp. 28 541–28 564, 2023.
- [14] M. S. Seyfioglu, W. O. Ikezogwo, F. Ghezloo, R. Krishna, and L. Shapiro, “Quilt-llava: Visual instruction tuning by extracting localized narratives from open-source histopathology videos,” in *Proceedings of the IEEE/CVF Conference on Computer Vision and Pattern Recognition*, 2024, pp. 13 183–13 192.
- [15] Y. Sun, Y. Zhang, Y. Si, C. Zhu, K. Zhang, Z. Shui, J. Li, X. Gong, X. LYU, T. Lin, and L. Yang, “Pathgen-1.6m: 1.6 million pathology image-text pairs generation through multi-agent collaboration,” in *The Thirteenth International Conference on Learning Representations*, 2025. [Online]. Available: <https://openreview.net/forum?id=rFpZnn11gj>
- [16] W. Ikezogwo, S. Seyfioglu, F. Ghezloo, D. Geva, F. Sheikh Mohammed, P. K. Anand, R. Krishna, and L. Shapiro, “Quilt-1m: One million image-text pairs for histopathology,” *Advances in neural information processing systems*, vol. 36, pp. 37 995–38 017, 2023.
- [17] Z. Huang, F. Bianchi, M. Yuksekgonul, T. J. Montine, and J. Zou, “A visual–language foundation model for pathology image analysis using medical twitter,” *Nature medicine*, vol. 29, no. 9, pp. 2307–2316, 2023.

- [18] S. Gunasekar, Y. Zhang, J. Aneja, C. C. T. Mendes, A. D. Giorno, S. Gopi, M. Javaheripi, P. Kauffmann, G. de Rosa, O. Saarikivi, A. Salim, S. Shah, H. S. Behl, X. Wang, S. Bubeck, R. Eldan, A. T. Kalai, Y. T. Lee, and Y. Li, “Textbooks are all you need,” 2023. [Online]. Available: <https://arxiv.org/abs/2306.11644>
- [19] D. Guo, D. Yang, H. Zhang, J. Song, R. Zhang, R. Xu, Q. Zhu, S. Ma, P. Wang, X. Bi *et al.*, “Deepseek-r1: Incentivizing reasoning capability in llms via reinforcement learning,” *arXiv preprint arXiv:2501.12948*, 2025.
- [20] Q. Team, “Qwq-32b: Embracing the power of reinforcement learning,” March 2025. [Online]. Available: <https://qwenlm.github.io/blog/qwq-32b/>
- [21] K. Team, A. Du, B. Gao, B. Xing, C. Jiang, C. Chen, C. Li, C. Xiao, C. Du, C. Liao *et al.*, “Kimi k1. 5: Scaling reinforcement learning with llms,” *arXiv preprint arXiv:2501.12599*, 2025.
- [22] W. Huang, B. Jia, Z. Zhai, S. Cao, Z. Ye, F. Zhao, Z. Xu, Y. Hu, and S. Lin, “Vision-r1: Incentivizing reasoning capability in multimodal large language models,” *arXiv preprint arXiv:2503.06749*, 2025.
- [23] Y. Lai, J. Zhong, M. Li, S. Zhao, and X. Yang, “Med-r1: Reinforcement learning for generalizable medical reasoning in vision-language models,” *arXiv preprint arXiv:2503.13939*, 2025.
- [24] J. Pan, C. Liu, J. Wu, F. Liu, J. Zhu, H. B. Li, C. Chen, C. Ouyang, and D. Rueckert, “Medvlm-r1: Incentivizing medical reasoning capability of vision-language models (vlms) via reinforcement learning,” *arXiv preprint arXiv:2502.19634*, 2025.
- [25] Z. Liu, X. Guo, F. Lou, L. Zeng, J. Niu, Z. Wang, J. Xu, W. Cai, Z. Yang, X. Zhao, C. Li, S. Xu, D. Chen, Y. Chen, Z. Bai, and L. Zhang, “Fin-r1: A large language model for financial reasoning through reinforcement learning,” 2025. [Online]. Available: <https://arxiv.org/abs/2503.16252>
- [26] Q. Yu, Z. Zhang, R. Zhu, Y. Yuan, X. Zuo, Y. Yue, T. Fan, G. Liu, L. Liu, X. Liu *et al.*, “Dapo: An open-source llm reinforcement learning system at scale,” *arXiv preprint arXiv:2503.14476*, 2025.
- [27] S. Eslami, C. Meinel, and G. De Melo, “Pubmedclip: How much does clip benefit visual question answering in the medical domain?” in *Findings of the Association for Computational Linguistics: EACL 2023*, 2023, pp. 1181–1193.
- [28] S. Zhang, Y. Xu, N. Usuyama, H. Xu, J. Bagga, R. Tinn, S. Preston, R. Rao, M. Wei, N. Valluri *et al.*, “A multimodal biomedical foundation model trained from fifteen million image–text pairs,” *NEJM AI*, vol. 2, no. 1, p. A10a2400640, 2025.
- [29] M. U. Khattak, S. Kunhimon, M. Naseer, S. Khan, and F. S. Khan, “Unimed-clip: Towards a unified image-text pretraining paradigm for diverse medical imaging modalities,” *arXiv preprint arXiv:2412.10372*, 2024.
- [30] K. Singhal, S. Azizi, T. Tu, S. S. Mahdavi, J. Wei, H. W. Chung, N. Scales, A. Tanwani, H. Cole-Lewis, S. Pfohl *et al.*, “Large language models encode clinical knowledge,” *Nature*, vol. 620, no. 7972, pp. 172–180, 2023.
- [31] J. Chen, C. Gui, R. Ouyang, A. Gao, S. Chen, G. Chen, X. Wang, Z. Cai, K. Ji, X. Wan *et al.*, “Towards injecting medical visual knowledge into multimodal llms at scale,” in *Proceedings of the 2024 Conference on Empirical Methods in Natural Language Processing*, 2024, pp. 7346–7370.
- [32] M. Y. Lu, B. Chen, D. F. Williamson, R. J. Chen, I. Liang, T. Ding, G. Jaume, I. Odintsov, L. P. Le, G. Gerber *et al.*, “A visual-language foundation model for computational pathology,” *Nature Medicine*, vol. 30, no. 3, pp. 863–874, 2024.
- [33] J. Xiang, X. Wang, X. Zhang, Y. Xi, F. Eweje, Y. Chen, Y. Li, C. Bergstrom, M. Gopaulchan, T. Kim *et al.*, “A vision–language foundation model for precision oncology,” *Nature*, pp. 1–10, 2025.
- [34] T. Ding, S. J. Wagner, A. H. Song, R. J. Chen, M. Y. Lu, A. Zhang, A. J. Vaidya, G. Jaume, M. Shaban, A. Kim *et al.*, “Multimodal whole slide foundation model for pathology,” *arXiv preprint arXiv:2411.19666*, 2024.
- [35] Y. Sun, C. Zhu, S. Zheng, K. Zhang, L. Sun, Z. Shui, Y. Zhang, H. Li, and L. Yang, “Pathasst: A generative foundation ai assistant towards artificial general intelligence of pathology,” in *Proceedings of the AAAI Conference on Artificial Intelligence*, vol. 38, no. 5, 2024, pp. 5034–5042.
- [36] M. Y. Lu, B. Chen, D. F. Williamson, R. J. Chen, M. Zhao, A. K. Chow, K. Ikemura, A. Kim, D. Pouli, A. Patel *et al.*, “A multimodal generative ai copilot for human pathology,” *Nature*, vol. 634, no. 8033, pp. 466–473, 2024.
- [37] Y. Sun, Y. Si, C. Zhu, X. Gong, K. Zhang, P. Chen, Y. Zhang, Z. Shui, T. Lin, and L. Yang, “Cpath-omni: A unified multimodal foundation model for patch and whole slide image analysis in computational pathology,” *arXiv preprint arXiv:2412.12077*, 2024.
- [38] D. Dai, Y. Zhang, L. Xu, Q. Yang, X. Shen, S. Xia, and G. Wang, “Pa-llava: A large language-vision assistant for human pathology image understanding,” in *2024 IEEE International Conference on Bioinformatics and Biomedicine (BIBM)*. IEEE, 2024, pp. 3138–3143.



- [39] A. Jaech, A. Kalai, A. Lerer, A. Richardson, A. El-Kishky, A. Low, A. Helyar, A. Madry, A. Beutel, A. Carney *et al.*, “Openai o1 system card,” *arXiv preprint arXiv:2412.16720*, 2024.
- [40] G. Xu, P. Jin, H. Li, Y. Song, L. Sun, and L. Yuan, “Llava-cot: Let vision language models reason step-by-step,” 2024. [Online]. Available: <https://arxiv.org/abs/2411.10440>
- [41] O. Thawakar, D. Dissanayake, K. More, R. Thawkar, A. Heakl, N. Ahsan, Y. Li, M. Zumri, J. Lahoud, R. M. Anwer *et al.*, “Llamav-o1: Rethinking step-by-step visual reasoning in llms,” *arXiv preprint arXiv:2501.06186*, 2025.
- [42] Z. Liu, Z. Sun, Y. Zang, X. Dong, Y. Cao, H. Duan, D. Lin, and J. Wang, “Visual-rft: Visual reinforcement fine-tuning,” *arXiv preprint arXiv:2503.01785*, 2025.
- [43] H. Shen, P. Liu, J. Li, C. Fang, Y. Ma, J. Liao, Q. Shen, Z. Zhang, K. Zhao, Q. Zhang *et al.*, “Vlm-r1: A stable and generalizable r1-style large vision-language model,” *arXiv preprint arXiv:2504.07615*, 2025.
- [44] E. Yu, K. Lin, L. Zhao, J. Yin, Y. Wei, Y. Peng, H. Wei, J. Sun, C. Han, Z. Ge *et al.*, “Perception-r1: Pioneering perception policy with reinforcement learning,” *arXiv preprint arXiv:2504.07954*, 2025.
- [45] Y. Yang, X. He, H. Pan, X. Jiang, Y. Deng, X. Yang, H. Lu, D. Yin, F. Rao, M. Zhu *et al.*, “R1-onevision: Advancing generalized multimodal reasoning through cross-modal formalization,” *arXiv preprint arXiv:2503.10615*, 2025.
- [46] L. Chen, L. Li, H. Zhao, Y. Song, and Vinci, “R1-v: Reinforcing super generalization ability in vision-language models with less than \$3,” <https://github.com/Deep-Agent/R1-V>, 2025, accessed: 2025-02-02.
- [47] Z. Zhao, H. Kang, B. Wang, and C. He, “Doclayout-yolo: Enhancing document layout analysis through diverse synthetic data and global-to-local adaptive perception,” 2024. [Online]. Available: <https://arxiv.org/abs/2410.12628>
- [48] J. Parmar, S. Satheesh, M. Patwary, M. Shoneybi, and B. Catanzaro, “Reuse, don’t retrain: A recipe for continued pretraining of language models,” *arXiv preprint arXiv:2407.07263*, 2024.
- [49] D. Cheng, S. Huang, and F. Wei, “Adapting large language models to domains via reading comprehension,” 2024. [Online]. Available: <https://arxiv.org/abs/2309.09530>
- [50] M. Tan and Q. Le, “EfficientNet: Rethinking model scaling for convolutional neural networks,” in *Proceedings of the 36th International Conference on Machine Learning*, ser. Proceedings of Machine Learning Research, K. Chaudhuri and R. Salakhutdinov, Eds., vol. 97. PMLR, 09–15 Jun 2019, pp. 6105–6114. [Online]. Available: <https://proceedings.mlr.press/v97/tan19a.html>
- [51] Z. Zhang, A. Zhang, M. Li, and A. Smola, “Automatic chain of thought prompting in large language models,” in *The Eleventh International Conference on Learning Representations*, 2023. [Online]. Available: <https://openreview.net/forum?id=5NTt8GFjUHkr>
- [52] J. Gamper and N. Rajpoot, “Multiple instance captioning: Learning representations from histopathology textbooks and articles,” in *Proceedings of the IEEE/CVF Conference on Computer Vision and Pattern Recognition (CVPR)*, June 2021, pp. 16 549–16 559.
- [53] J. Silva-Rodríguez, “Sicapv2-prostate whole slide images with gleason grades annotations,” *Mendeley Data*, 2020.
- [54] C. Han, X. Pan, L. Yan, H. Lin, B. Li, S. Yao, S. Lv, Z. Shi, J. Mai, J. Lin *et al.*, “Wsss4luad: Grand challenge on weakly-supervised tissue semantic segmentation for lung adenocarcinoma,” *arXiv preprint arXiv:2204.06455*, 2022.
- [55] A. A. Borkowski, M. M. Bui, L. B. Thomas, C. P. Wilson, L. A. DeLand, and S. M. Mastorides, “Lung and colon cancer histopathological image dataset (lc25000),” *arXiv preprint arXiv:1912.12142*, 2019.
- [56] E. C. Welch, C. Lu, C. J. Sung, C. Zhang, A. Tripathi, and J. Ou, “Bmt: A cross-validated thinprep pap cervical cytology dataset for machine learning model training and validation,” *Scientific Data*, vol. 11, no. 1, p. 1444, 2024.
- [57] H. Duan, J. Yang, Y. Qiao, X. Fang, L. Chen, Y. Liu, X. Dong, Y. Zang, P. Zhang, J. Wang *et al.*, “Vlmevalkit: An open-source toolkit for evaluating large multi-modality models,” in *Proceedings of the 32nd ACM International Conference on Multimedia*, 2024, pp. 11 198–11 201.
- [58] S. Xu, W. Xie, L. Zhao, and P. He, “Chain of draft: Thinking faster by writing less,” *arXiv preprint arXiv:2502.18600*, 2025.
- [59] Y. Sun, H. Wu, C. Zhu, S. Zheng, Q. Chen, K. Zhang, Y. Zhang, D. Wan, X. Lan, M. Zheng *et al.*, “Pathmmu: A massive multimodal expert-level benchmark for understanding and reasoning in pathology,” in *European Conference on Computer Vision*. Springer, 2024, pp. 56–73.
- [60] Y. Zuo, S. Qu, Y. Li, Z. Chen, X. Zhu, E. Hua, K. Zhang, N. Ding, and B. Zhou, “Medxpertqa: Benchmarking expert-level medical reasoning and understanding,” *arXiv preprint arXiv:2501.18362*, 2025.
- [61] Y. Hu, T. Li, Q. Lu, W. Shao, J. He, Y. Qiao, and P. Luo, “Omnimedvqa: A new large-scale comprehensive evaluation benchmark for medical lvlm,” in *Proceedings of the IEEE/CVF Conference on Computer Vision and Pattern Recognition*, 2024, pp. 22 170–22 183.